An Annual Model of a Solar-Hydrogen Energy Storage System

Brendan A. McCormick, Stephen J. Harrison, Jon G. Pharoah
Department of Mechanical & Materials Engineering, Queen's University
Kingston, Ontario
brendan.mccormick@queensu.ca harrison@me.queensu.ca pharoah@me.queensu.ca

ABSTRACT

This study is a preliminary assessment of the sizing, energy flows, and round-trip efficiency of a solar-powered water electrolysis system. The simulated system demonstrates the potential to operate autonomously from the electricity grid. Hydrogen gas is produced during peak solar hours and stored for later use in a fuel cell. The fuel cell delivers power at times of low solar availability. This study found that a hybrid system, combining battery and hydrogen gas storage, could meet an annual load demand of 4800 kWh. The system uses a 5.9 kWp solar array, a 20 kW PEM electrolyzer, a 3.7 kWp PEM fuel cell, and an 1800 Ah battery bank. The overall hydrogen-loop energy efficiency is 6.1%, from PV conversion to re-electrification of H_2 in the fuel cell.

INTRODUCTION

Solar power generation in Ontario has seen great advancements in the last decade, with significant penetration into domestic/residential markets. The use of incentives (FeedInTariff program [1]), and the development of cost effective roof-top mounting has driven this. While distributed generation of electric power has become commonplace, distributed energy storage technologies have received less attention. Storage is known to be a key component of the wide-scale adoption of renewable energy. Practical energy storage is essential for matching intermittent production of renewable power with the time dependent power demand of residences.

Several options for energy storage currently exist, including mechanical forms of storage in flywheel and pumped water storage, or chemical forms of storage in batteries and hydrogen gas. Many of these storage systems have been developed and demonstrated in commercial settings for many years [2]. Some newer forms of storage, such as ultracapcitance, are emerging but are still impractical technologies [3].

The focus of this study was to model the production, storage, and use of hydrogen gas. The method of production is through solar-powered water electrolysis. Excess solar power is directed to a proton exchange membrane (PEM) electrolyzer, producing H_2 gas to be stored at relatively low pressure for later use in a PEM fuel cell. The hydrogen system works in conjunction with a battery bank to meet the load demand of a typical Canadian home as described by Armstrong et al. [4].

BACKGROUND & RELATED WORK

An electrolyzer is a device that, through the application of a voltage across two electrodes separated by an electrolyte, splits water molecules into hydrogen and oxygen gases.

Two technologies make up the majority of the water electrolysis market; alkaline electrolysis and proton exchange membrane electrolysis. Alkaline electrolyzers have two electrodes submerged in a liquid electrolyte. These are separated by a diaphragm that is used to keep the product gases of hydrogen and oxygen apart. A PEM electrolyzer employs a solid Nafion® membrane as the electrolyte, which, due to its solid nature, also acts as a diaphragm. H^+ ions, produced on a catalyst layer adjacent to the membrane, can be pulled through the membrane, while oxygen gas cannot. Nafion is a polymer developed by DuPont, and thus proton exchange membranes have also been called polymer electrolyte membranes.

While they are a well-established commercial technology, alkaline electrolyzers face challenges when used in renewable energy systems. These issues include low efficiency at partial loads, low current density limits, and low operating pressures [5]. Current density is limited by the high ohmic losses across the liquid electrolyte and diaphragm. Diaphragms in alkaline electrolysis do a poor job of preventing gas diffusion. Oxygen gas can diffuse into the cathode chamber, recombining with the H_2 gas and reducing the overall efficiency. Likewise, H_2 can diffuse into the anode chamber posing a safety risk.

A PEM electrolyzer offers the ability to operate at much higher current densities due to the high proton conductivity across the thin solid membrane (i.e., low ohmic losses). Gas cross-over is limited due to the low permeability of the Nafion membrane, thus allowing the PEM to operate under a wide-range of power inputs [6].

PEM electrolyzers and fuel cells demonstrate rapid response to the transient operating conditions observed in a renewable energy power supply and household power demand. PEM electrolyzers have been shown to have response times well below one second for both 75% increases, and decreases, in power supplied [7]. PEM fuel cells show a similarly rapid response rate, well below one second for major increases in current demand (50% increase) [8].

Experimental Efforts

Examples of experimental solar-hydrogen energy systems date back to the 1970's, when the first lab scale experiments were conducted [9] [10]. Solar arrays and electrolyzer cells were directly coupled (i.e., with no power conditioning between them). The performance curves of the two devices were matched by varying the series-parallel stacking of the cells in both the solar array and electrolyzer.

In the early 1990's the first residential systems began to appear. In Switzerland, a 5 kWp solar array was connected with conditioning devices to a 5 kW alkaline electrolyzer. Hydrogen was stored in a 15 Nm^3 (normal meter cubed) metal hydride storage tank. Hydrogen gas was used to operate household appliances that were able to run on hydrogen, and for a hydrogen mini-bus. The system could produce 1100 Nm^3/year, corresponding to a 3.6% efficiency for converting solar radiation into hydrogen fuel [11].

In a later study, a research home in Germany utilized a 4.2 kWp solar array to charge a 20 kWh capacity battery bank and a 2 kW PEM electrolyzer. The hydrogen produced was combusted for space heating and cooking, and used to power a 1 kW fuel cell. In combination with a solar thermal collector, ventilation heat recovery, and highly efficient insulation, the system was able to supply the entire annual energy demand of the dwelling (3 person, 145 m^2, 1740 kWh/year) [12].

Larger commercial systems have since been built, with one of the largest located on the island of Utsira, Norway [13]. As wind is abundant in this location, a 600 kW wind turbine was used instead of a solar array. The inherent variability of the wind power supply resulted in this system facing similar problems as a solar powered system and therefore, these two systems are subject to the same challenges. In this system, the wind turbine delivered power to a low voltage mini-grid that supplied 10 homes with power. Excess power was directed to a 50 kW alkaline electrolyzer to produce H_2 gas that was mechanically compressed and stored in a 2400 Nm^3 tank. A 10 kW fuel cell or 55 kW hydrogen combustion engine provided auxiliary power when the wind supply was insufficient to meet demand. The system was designed to provide 2-3 days of full energy autonomy for the island, and over the course of one month was able to supply 50% of the required demand. Modelling was performed by the authors to determine what changes could be made to improve system performance. It was found that the combination of a 300% increase in storage tank size and replacement of the hydrogen engine with a fuel cell of similar size could achieve full energy autonomy over the studied month. The simulation tool used was TRNSYS.

These experimental efforts demonstrate successful design and operation of solar-hydrogen energy systems, and this study aims to expand on the development of real systems by creating a simulation that can test different system sizes and environments, and that reflects changes in electrolyzer technology.

MODEL DEVELOPMENT & SIMULATION

The system models used in this study are written as FORTRAN subroutines, designed to run with the simulation program TRNSYS. TRNSYS is a simulation environment for the transient simulation of systems. The TRNSYS library includes many of the components necessary to design renewable energy systems (referred to as Component "TYPES"), as well as routines to input weather data and other time-dependent forcing functions. Its open and modular structure allows for users to easily extend existing models to make them fit specific needs.

General Model Description

The typical architecture of a solar hydrogen energy system can be seen in Fig. 1, with the specific architecture of the studied system found in Fig. 2.

A solar array was simulated based on a 5 parameter model [14] as implemented in TRNSYS Type 94. The solar array delivers power to a system controller Type48, that distributes power to a battery bank (Type 47b), electrolyzer (Type 160b), and load. The battery bank was modelled with a charge and discharge current limit, so as to protect the battery from overheating and gas-off, and deep discharges. The battery system went through a daily charge/discharge cycle. The lower SOC limit placed on the battery bank was 60%, a common limit for deep-cycle batteries. While the battery system is non-essential for the simulated system to work, real systems described in literature require the battery bank to stabilize the common DC bus that would exist between all the components [21]. It was therefore necessary to simulate the power flows into and out of the batteries.

The solar array was oversized relative to the capacity of the battery bank, which would result in excess power being produced by the system. During these times, this excess power is directed to the electrolyzer. The power is first sent through a conditioning device to match the voltage level to the electrolyzer operating voltage. The resulting current is delivered to the electrolyzer and used to produce H_2 gas. The gas is mechanically compressed in a 3-stage compressor, (the power consumption is fed back to the load file), and stored in a 14 bar pressure vessel. The behavior of the hydrogen gas stored within the tank is modelled using Van-DerWahls equations for real gases.

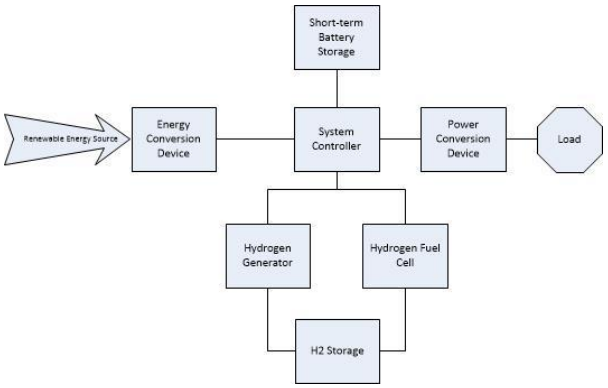

Figure 1: General architecture of a solar-hydrogen energy system.

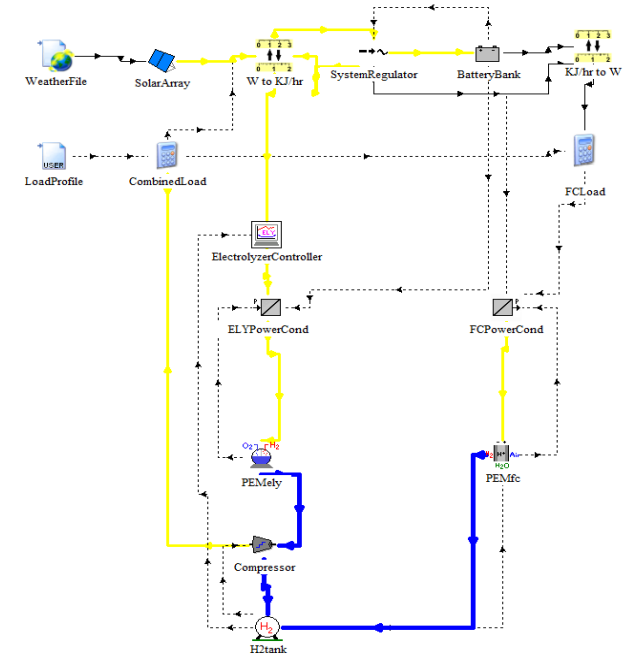

Figure 2: Graphic representation of the simulated system in TRNSYS (i.e., Screen-capture). Yellow represents flows of electric power, blue shows flows of hydrogen gas, and dashed lines are signals.

This pressurized tank feeds a PEM fuel cell (Type 170b) to produce power when power from the batteries is insufficient to meet the desired load.

Weather Data & Building Load

The weather data used was CWECS data for Toronto, ON. The data used for modelling the building electrical load was provided by Marianne Armstrong, of the National Research Council, Canada. This load profile is representative of the occupancy patterns in a Canadian home that has a low electrical demand relative to the Canadian average. The load represents major appliances in the home (fridge, freezer, stove, dryer, etc.) as well as more minor appliances (toaster, hair dryer, drill, etc.). The authors of the study synthetically derived the load profile and compared it with consumption data from by Hydro Quebec. The derivation and comparison is described in [4]. Figure 3 shows one week of the synthetic load profile, matched with a CWECS weather data file of available solar energy at the same time of year, in Toronto, Ontario.

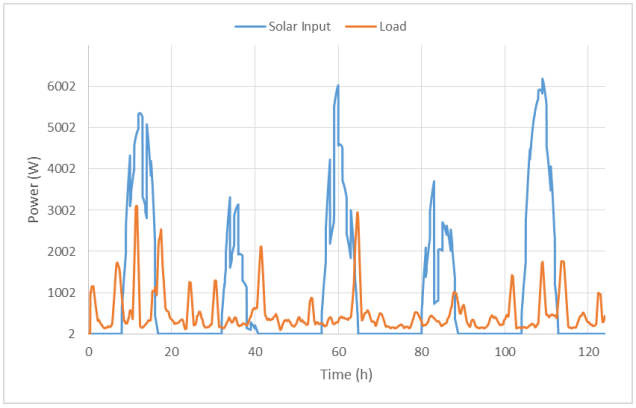

Figure 3: Synthetic load profile matched with available solar energy for a 1-week period.

The original dataset was smoothed using a 10-point moving average. This was necessary to promote convergence of the TRNSYS model, as large swings in power demand caused non-convergence in the fuel cell and power conditioner models. The average load demand over the entire dataset is 543 W, with a peak demand of 6416 W. After smoothing, the largest transients were constrained to 120 W/min for the purpose of system modelling.

Component Modelling

This section focuses on the theory behind the modeling of a PEM electrolyzer and fuel cell in TRNSYS. Other components used (such as solar arrays, batteries, charge controllers, power conditioning devices, etc.) are not explored as rigorously.

The main FORTRAN frameworks for the electrolyzer and fuel cell models were developed by Øystein Ulleberg at the Institute for Energy Technology, Kjeller, Norway. The models use basic thermodynamic and heat transfer principles to determine the rate of H_2 production/consumption and the thermal energy balance of the system, as described in [15]. This paper places greater emphasis on the modelling of the electrolyzer, as adaptation was required to reflect the performance of a PEM electrolyzer. The TRNSYS library already contains a validated air-breathing PEM fuel cell.

Electrolyzer Model

In a PEM electrolyzer, water is introduced at the anode and dissociated into oxygen, protons, and electrons. The protons are driven through the polymer electrolyte membrane under an electric field where they combine with electrons arriving from an external circuit to form hydrogen gas. From a thermodynamic perspective, the minimum voltage to start the water electrolysis reaction corresponds to the sum of the reversible potentials for each half-reaction at both electrodes [16]. Reversible potential is proportional to the Gibbs Free energy of the system, and inversely proportional to the charge transfer, *nF*:

$$U_{rev}^{0} = \frac{\Delta G^{0}}{nF} \qquad (1)$$

Anode: $H_2O \rightarrow 2H^+ + 1/2O_2 + 2e^-$

$U_{rev}^{0} = 1.229V$

Cathode: $2H^+ + 2e^- \rightarrow H_2$

$U_{rev}^{0} = 0.000V$

Total: $H_2O \rightarrow 2H_2 + 1/2O_2$

$U_{rev}^{0} = 1.229V$

This reversible voltage neglects the thermal energy demand for this reaction, $T\Delta S$. By calculating cell voltage based on a change in enthalpy, ΔH, one can determine the thermoneutral voltage of the reaction to be 1.48V. The thermoneutral voltage represents the combined electrical and thermal energy required for the reaction to proceed.

Real systems always require voltages higher than the reversible voltage due to internal resistances of the cell and kinetic losses. The operating voltage is therefore a sum of several over-potentials (i.e., losses), namely the cell's Nernst potential (i.e., open circuit voltage), and activation, ohmic, and mass transport losses. The summation of these over-potentials results in a performance curve for the cell, which demonstrates its operating voltage for a given current input. These over-potentials are affected by operating pressure and temperature, with temperature being the dominating affect [17].

A FORTRAN subroutine created by Ulleberg, Type 160, uses a temperature dependent relation to describe the performance curve of an electrolyzer which sums the various over-potentials, i.e.,

$$U = U_{rev}^{0} + \frac{r_1 + r_2 T}{A} I + s \log\left(\frac{t_1 + t_2/T + t_3/T^2}{A} I + 1\right) \qquad (2)$$

where U_{rev}^{o} is the reversible voltage, T is the cell temperature, I is the stack current, A is the stack area, and r_1, r_2, s, t_1, t_2, and t_3 are empirically determined constants. These constants are supplied to the TRNSYS routine in an external file that can be edited by the user. These constants determine the shape of the polarization curve, and were originally intended to describe the performance of an alkaline cell.

For this study, new constants had to be determined to accurately model the PEM electrolyzer. Performance data in the form of a polarization curve was supplied by *Proton OnSite*, a PEM electrolyzer manufacturer. This polarization curve was digitized using a plot digitizer and then processed in Engineering Equation Solver (EES) to curve fit the data to an equation of the form shown in Eq. 2.

The difference in performance curves between the alkaline and PEM electrolyzers at 80°C is shown in Fig. 4:

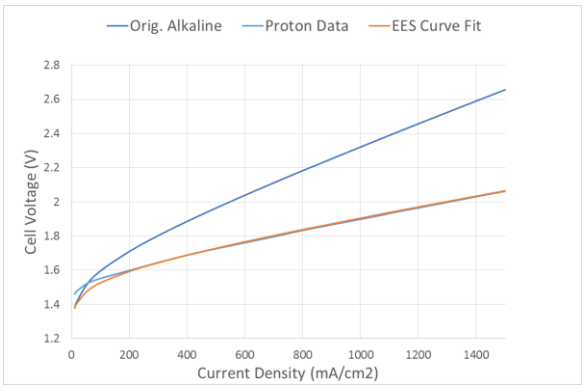

Figure 4: Comparison of manufacturer's data and EES curve fit results.

This new performance curve could now be used to determine the operating voltage for a specific current input, and thus determine the voltage efficiency of the cell, defined as,

$$\eta_V = \frac{U_{tn}}{U_{cell}} \quad (3)$$

where U_{tn} is the thermoneutral voltage, and U_{cell} is the measured operating voltage of the cell. This efficiency is used to calculate the rate of thermal energy generated by the electrolyzer, as seen in,

$$Q_{gen} = P_{in}(1-\eta_V) \quad (4)$$

where P_{in} is the power input into the electrolyzer. This heat generation value is used in a thermal energy balance:

$$Q_{gen} = Q_{store} + Q_{loss} + Q_{cool} \quad (5)$$

The model maintains a steady cooling water flowrate, and allows the electrolyzer temperature to fluctuate between room temperature and a maximum operating temperature of 100°C.

Based on Faradays law, the production rate of hydrogen in an electrochemical cell is,

$$\dot{n}_{H2} = \frac{I}{nF} \quad (6)$$

where the production rate (in moles) of hydrogen gas is proportional to the applied current I, and inversely proportional to the number of electrons transferred, n, multiplied by Faraday's constant. This number reflects the rate of hydrogen production if no losses were to occur. However, a real electrochemical cell will never produce the theoretical maximum amount of H_2. Therefore, the output must be modified, in order to compensate for this inefficiency, by the Faraday efficiency.

The Faraday efficiency is the ratio of the amount of H_2 produced by the cell to the final amount seen in the exit stream. A discrepancy also exists between these two amounts due to diffusion of species across the polymer membrane. Typically insignificant at low operating pressures (<10bar) [6], Schalenbach et al. demonstrated there is some efficiency loss due to gas crossover at low current densities [18]. As current density increases, Ohmic losses begin to dominate due to membrane resistivity. Because gas cross-over is more prevalent in an alkaline electrolyzer, a PEM cell usually has a higher Faraday efficiency. For this study, Type 160b was modified to reflect this affect. Ulleberg's model defined Faraday efficiency as,

$$\eta_F = \frac{j^2}{a_1 + j^2} a_2 \quad (7)$$

where j is the current density and a_1, and a_2 are empirically determined constants. The total efficiency of the PEM electrolyzer cell is then defined as:

$$\eta_e = \eta_V \times \eta_F \quad (8)$$

Using Schalenbach's results and the EES curve fitting tool, new constants for Eq. 7 were found. The results of the EES curve fit can be seen as the yellow line in Fig. 4. The curve matches Schalenbach's data well in the low current density region where the impacts of gas crossover are significant. The two curves diverge as current density increases due to differences in the *Ohmic* losses of each respective cell.

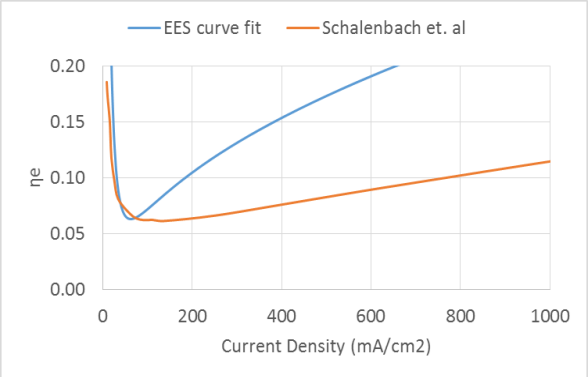

Figure 5: Comparison of Schalenbach's data and EES curve fit. The drastic divergence past 100mA/cm2 is due to differences in ohmic resistances of the cells, unrelated to the Faraday efficiency.

Fuel Cell Model Development

In an air-breathing PEM fuel cell, hydrogen and air are introduced separately at the anode (H_2) and cathode (air). H_2 atoms are catalyzed on the anode and H^+ ions are transported through the polymer membrane while electrons are forced around an external circuit. H^+ combines with O_2 and incoming electrons on the cathode side, forming H_2O. The calculation of the reversible and thermoneutral voltages is much the same as for a PEM electrolyzer. The same losses that affect an electrolyzer also impact a fuel cell, however these losses work to reduce the output voltage of the cell. Ulleberg's model determines the cell voltage, U_{cell}, through the summation of the reversible voltage and losses:

$$U_{cell} = U^0_{rev} - U_{act} - U_{ohmic} \quad (9)$$

The reversible voltage is determined using the Nernst equation which accounts for the concentration of species. The activation overvoltage is based on theoretical equations from kinetic, thermodynamic,

and electrochemistry fundamentals. The Ohmic over-voltage is purely empirical, based on temperature and current data.

The energy efficiency is calculated from the thermoneutral voltage and the cell voltage,

$$\eta_e = \frac{U_{cell}}{U_{tn}} \qquad (10)$$

This energy efficiency is used in the thermal model to determine the internal heat generation of the fuel cell,

$$Q_{gen} = P_{stack}\left[\frac{1-\eta_e}{\eta_e}\right] \qquad (11)$$

where P_{stack} is the fuel cell output power.

The consumption rate of H_2 gas is determined by Faraday's law (as in the case of the electrolyzer). Stoichiometric ratios are also considered, ensuring that there is a plentiful supply of H_2 to the unit.

RESULTS OF SIMULATION & DISCUSSION

The size of the solar-hydrogen system simulated can be seen in Table 1. The system was sized to produce a net positive gain in stored hydrogen over the course of the year.

Table 1: Solar-hydrogen system component sizing

Component	System Specs.
Solar Array	5.6 kWp, 236 V 23.4 A @MPP 45' slope
PEM Electrolyzer	20 kWp, Max Power Density: 4.4W/cm^2
PEM fuel cell	3.7 kWp
Battery Bank	48 V, 21.6kWh
Storage Tank	44m^3, 14 bar, 2000 kWh H_2 gas

Figure 9 shows the state of charge (SOC) of the H_2 storage tank over the period of the simulated year. Two equally sized systems are considered:

- A PEM electrolyzer system (blue line)
- An alkaline electrolyzer system (orange line)

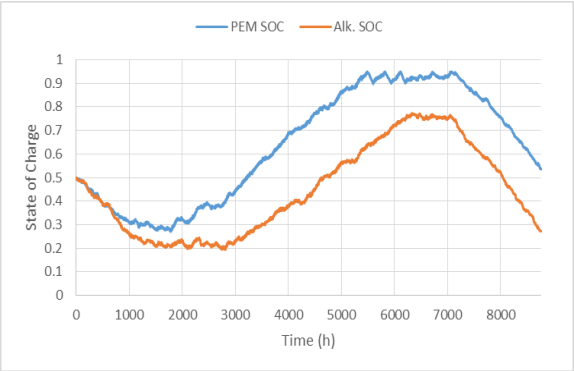

Figure 6: State of charge (SOC) of the hydrogen storage tank for 2 simulated systems; PEM electrolyzer (blue), and alkaline electrolyzer (orange)

The simulations begin with an initial hydrogen tank SOC of 50%. The PEM system outperforms the alkaline system, achieving a much higher end of year SOC. This is due to the higher Faraday efficiency of the PEM system, and the lower operating voltage.

For the PEM system, the minimum SOC reached was 27%, occurring at hour 1785 or March 15th in calendar time. The maximum SOC is reached several times due to the tank SOC limit (95%). The limit is reached for the first time at hour 5485 or August 16. It is reached twice more over the course of the year.

The peaks seen in Fig.7 are generated as the hydrogen storage tank reaches capacity. The electrolyzer ceases production at 95%SOC, and resumes operation once the SOC drops below 90%. While the hydrogen storage tanks are between these limits, a large portion of solar energy goes unutilized by the system. This amounted to 443 kWh of high grade electrical energy. Opportunity exists to harness this electrical energy for further use. The time of this excess coincides well with the annual peaks seen in the provincial electricity grid. Net-metering between the system and the grid could occur. Also of interest is the opportunity for the electricity to be used to generate hydrogen for use in a fuel cell vehicle.

Solar-Hydrogen System Performance

The system simulated was able to deliver 98% of the energy demanded by the load. The lack of full autonomy occurred during periods when the load demanded exceeded the power that could be delivered by either storage medium. The battery was either in a state of discharge, or the fuel cell was operating at maximum power output.

The major energy flows in the solar-hydrogen system can be seen in Table 2, as well as Fig. 7:

Table 2: Energy produced or consumed by each individual system component.

Component	Energy Produced/Consumed (kWh)
Solar Array Output	9198.2
Load	4826.1
Electrolyzer	5825.8
Fuel Cell	2429.4
Battery Charging	737.5
Battery Discharging	533.9
Gas Compressor	56.6

Figure 7 provides a visual representation of the summed annual energy flows through the system. Yellow and purple flows represent energy in the form of electricity. The purple flows indicate electricity that is passing through the hydrogen system. Green flows represent chemical energy in the form of hydrogen gas. The energy content of the gas was determined based on the heat of formation of liquid water, H_f= 286kJ/mol. While a significant proportion of the hydrogen gas is used by the fuel cell, a net surplus of gas exists at the end of the simulated year. This amounts to 601 kWh of chemical potential energy. Red flows represent flows of thermal energy through the system.

Over the course of the simulated year the solar array had an average efficiency of 12.6%. The hydrogen loop efficiency was found to be 48.7% for the 1 year period. The overall energy efficiency of the hydrogen loop was determined by comparing the energy flow into the electrolyzer's power conditioner with the energy produced by the fuel cell power conditioner and remaining in the storage tank at the end of the year. Combined with the average solar array efficiency, the hydrogen system efficiency from incident solar radiation to DC load delivered is 6.1%. The ratio of load delivered to solar array output is 52.5%

System efficiency could be further improved by making use of the flows of thermal energy in the system. Both the electrolyzer and fuel cell have flows of liquid water that remove thermal energy from the devices. The amount of energy and temperature of each stream seen in Table 3. The electrolyzer is cooled by the supply of deionized water to the stack assembly. The primary use for this water is to supply the electrochemical reaction, but it also doubles as a cooling loop due to the stoichiometric excess of the flow. This deionized water is at room temperature (20°C) upon entering the electrolyzer, and the TRNSYS results showed an average exit temperature of 23°C.

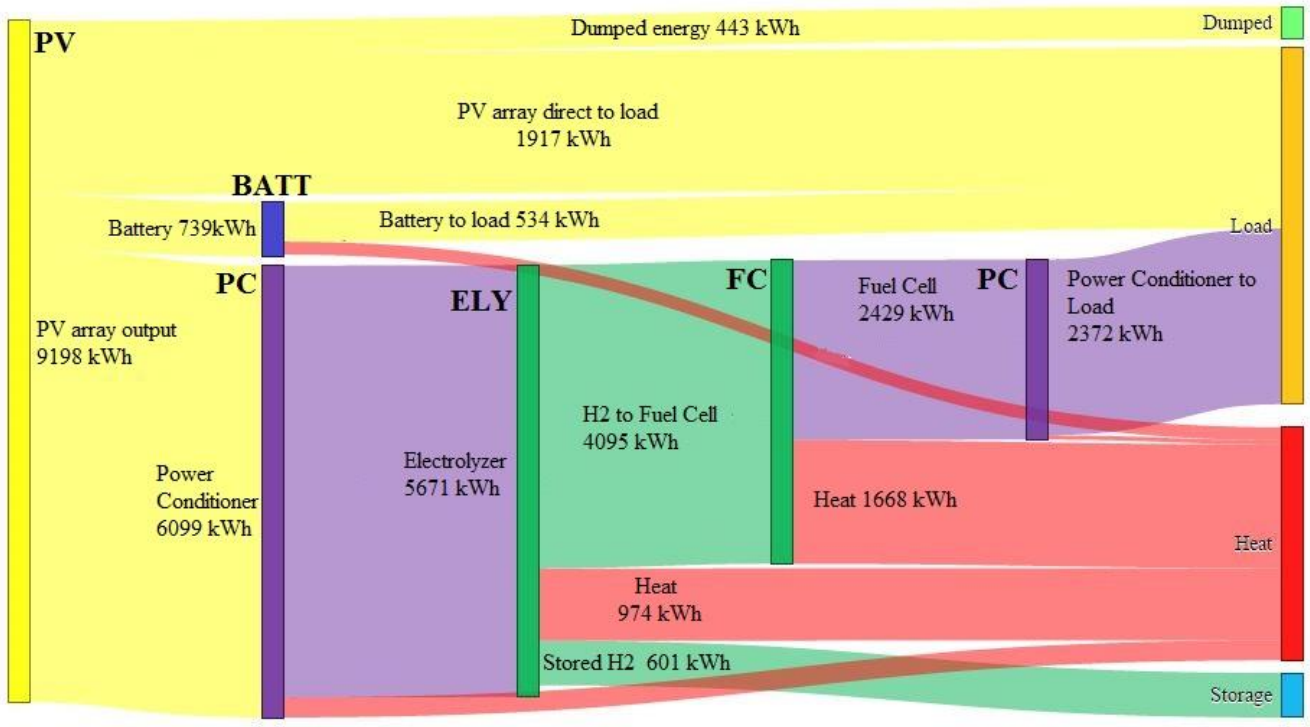

Figure 7: Energy flows through the solar-hydrogen energy storage system

The fuel cell requires an independent supply of cooling water to remove excess heat from the stack. This cooling water entered the fuel cell at mains water temperature, and exited at an average temperature of 43°C. Potential exists to capture this thermal energy for use in pre-heating a hot water supply, and will be the focus of future studies.

Table 3: Sources of heat in the solar-hydrogen system

Source of Heat	Thermal Energy (kWh)
Fuel Cell	1379 @ 43°C
Electrolyzer	318 @ 23°C
Electrolyzer Power Conditioner	269
Fuel Cell Power Conditioner	57

2.9% of the total solar energy input remains unaccounted for in the simulation. This can be attributed to discrepancies in the input and output energy of the battery and electrolyzer models. At this point in time, it is assumed that this unaccounted for energy is low-grade heat. Further investigation will be conducted to validate this assumption.

Convergence of the fuel cell and power conditioner models was an issue. The rapid swings in power demand caused input calculations to not converge over calculation periods. This was addressed by limiting the minimum cell voltage of the fuel cell to 0.5V. The authors found that convergence was promoted by maintaining the operating voltage above this point. Other attempts were made to change the simulation time step, and the control card component order to no avail.

All-Battery System

To identify benefits or shortcomings of the solar-hydrogen system, an all-battery system was also simulated. The all-battery system was sized to deliver the same load reliability that the solar-hydrogen system achieved, 98%. While this expectation might be high for a real-world simulation, this comparison requires both reliabilities to be the same.

The required battery bank size was determined by finding periods of time with low solar insolation and high load. During these periods, the net flow of energy out of the system is near a maximum. The battery bank was sized to deliver the required load for the most extreme of these periods. It was assumed that the battery would be at or near a full state of charge at the beginning of such a period. Once the battery bank size was determined, the solar array size was adjusted until the system could meet the 98% reliability criterion. Using a sensitivity analysis, one can see the impact the solar array size has on the overall reliability of the system:

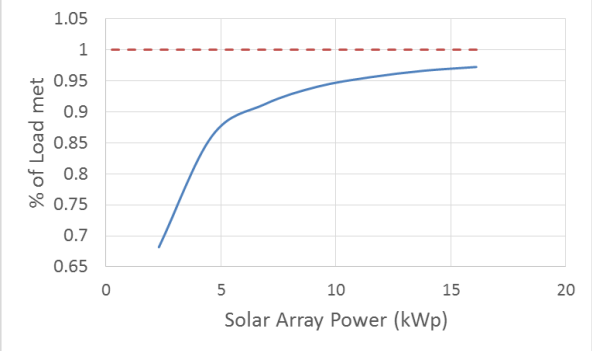

Figure 8: sensitivity analysis of solar array size for all-battery system

The final system size can be seen Table 4, compared with the component sizes of the solar-hydrogen system.

Table 4: Comparison of S-H and all battery system sizes

Component	S-H System	Battery System
Solar Array	5.6 kWp, 236 V 23.4 A @MPP, 45’ slope	11.5 kWp, 294.9 V 39 A @MPP, 45’ slope
PEM Electrolyzer	20 kWp, Max Power Density: 4.4W/cm^2	
PEM fuel cell	3.7 kWp	
H_2 Storage	44m^3, 2000kWh	
Battery Bank	48 V, 21.6kWh	48V, 172.8kWh

The required battery bank would consist of 24 strings of 4 series-connected 12V batteries, or 96 deep-cycle batteries in total. The battery technical specifications were taken from a data sheet for the Outback 170RE battery [19]. Each battery has a 150Ah storage capacity at a C-rate of 5 hours (C5). The discharge current is limited to ensure the C-rate does not exceed 5 hours. This limits the discharge current to 30A for each

battery string. An increase in C-rate (4 hours, 3 hours, etc.) results in a decrease in capacity, and thus, the requirement for a larger battery array. C-5 was chosen based on the manufacturer's recommendation [19]. Likewise, the charge rate was limited to 40A per battery string to prevent overheating of the battery cells during charging, based on the manufacturer's recommendation. The minimum SOC of the battery array was 60%, corresponding to a cell voltage of 1.8V. Discharge beyond this point was not allowed, based on recommendations from the manufacturer [20].

The required solar array size is larger than in the solar-hydrogen system. This is necessary to ensure the battery bank reaches an appropriate level of charge to meet the load demand at night, and other periods of low solar insolation.

Table 5: Energy consumed/produced by each system component in the all-battery system

Component	Energy Produced/Consumed (kWh)
Solar Array	19162.9
Load	4769.5
Battery Charging	3375.4
Battery Discharging	2656.3

Fig. 9 shows the summed annual flow of energy through the all-battery system. The largest portion of the energy flow goes unutilized, nearly 72% (dumped). This dumping occurs when the battery bank is in a full state of charge and the load is being met. The additional solar capacity is required to charge the bank in an acceptable time period (~6hrs), but once the bank reaches a full charge the power is no longer required.

The load receives 11% of the solar input directly, and 18% is sent to the battery to be stored. A large portion of output from the PV array goes unused.

The battery array demonstrated a charge/discharge efficiency of 79%.

Comparison between the Systems

The comparison is limited to technical aspects of both systems. Economic comparison is beyond the scope of this paper at this time.

The battery and solar-hydrogen systems designs both offer advantages and disadvantages. The S-H design has an inherent complexity when compared to the all-battery system, due to the addition of the hydrogen loop. The loop requires another layer of controls to manage the power flows through the system. A trade-off exists between this increased complexity and the additional flexibility this controls system affords. The controllers can be modified to react differently when certain thresholds are exceeded. This will become important when the transient effects of the electrolyzer and fuel cell are studied more closely. The two systems

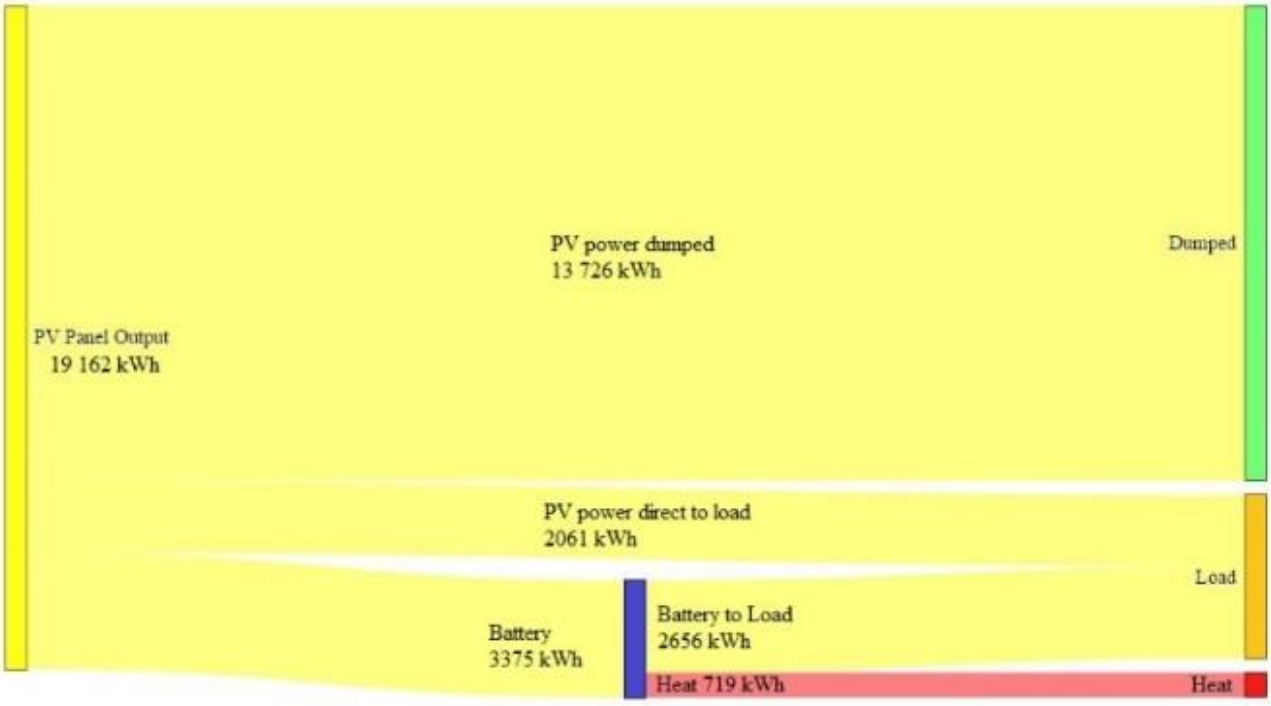

Figure 9: Sankey diagram of energy flows in the all-battery system. Note the large portion of solar energy that goes unused.

could see improvements on overall lifetime by allowing more constant operation.

While both systems have flows of thermal energy, the S-H system offers a more readily accessible source of thermal energy. The main source, from the fuel cell cooling loop, is contained within a flow of cooling water that can be passed through an additional heat exchanger, extracting the thermal energy for further use. The high temperature of this heat source offers opportunities for water pre-heating.

The battery array is recommended to have a cooling system to maintain the environmental temperature limit of 25°C (the working fluid of this system being air) [20]. With a forced convection system outputting air at a temperature of 25°C, the use of this thermal energy is practically limited to space heating.

Considering the storage volume, the battery system has a size advantage over the S-H system. Using the manufacturer's specs and recommended battery spacing, the bank would occupy 0.8m^3. Compared to the 44m^3 hydrogen storage tanks, the battery bank occupies a significantly smaller footprint. Changes in hydrogen storage (higher pressure, metal hydride) are required to improve this technical aspect of the solar-hydrogen system.

Considering the array size, the solar-hydrogen system has a 5.6kWp solar array; the all-battery system has an array twice that size (11.5kWp). This larger array is necessary to charge the batteries in a short enough time period and to a sufficient level, before power is drawn from them again. The solar array must also meet the load demand while the batteries are charging.

CONCLUSIONS

A model of a residential scale solar-powered water electrolysis system was developed. The model uses CWECS weather data for Toronto, Ontario, and a synthetically derived load profile representative of a low energy dwelling as inputs. This paper presents an adequately sized solar array, PEM-based hydrogen energy storage system, and battery bank to meet this electrical energy demand. The system was analyzed to understand the energy flows and identify useful secondary energy flows. Of particular interest is the waste heat generated by the fuel cell, which can act as a significant source of thermal heating for the dwelling. The system was compared to the performance of an equally sized alkaline electrolyzer system, and an all-battery system. The all-battery system was seen to be a more attractive option from a volume and efficiency perspective, but does not offer the same benefit of waste heat streams.

A PEM electrolyzer system was shown to have better theoretical performance than a system based on an alkaline electrolyzer. The PEM electrolyzer benefits from a higher Faraday efficiency and lower operating voltages.

The size of system required to meet the dwelling's demand is reasonable for residential application, consisting of a 5.9kWp solar array, a 20kW electrolyzer, and a 3.7kW fuel cell. The size of the required storage devices are a 44 m^3 pressure vessel with a pressure rating of 1.4MPa, and 12 deep cycle lead acid batteries.

The system would benefit from further optimization. Using a genetic algorithm optimization and appropriate cost functions, further decrease in the overall size could be achieved.

The current energy hierarchy prioritizes battery charging and discharging before hydrogen production and consumption. A new controller logic should be developed to investigate alternative energy system hierarchies.

ACKNOWLEDGEMENTS

The authors would like to acknowledge the support of the NSERC Smart Net Zero Energy Buildings Strategic Research Network (SNEBRN).

REFERENCES

[1] L. Stokes, "The politics of renewable energy policy: The case of feed-in tariffs in Ontario, Canada," Energy Policy, vol. 56, pp. 490-500, 2013.

[2] H. Chen and T. Cong, "Progress in electrical energy storage system: A critical review," Progress in Natural Science, no. 19, pp. 291-312, 2009.

[3] J. Maclay, J. Brouwer and G. Samuelson, "Dynamic modeling of hybrid energy storage systems coupled to photovoltaic generation in residential applications," Journal of Power Sources, no. 163, pp. 916-925, 2007.

[4] M. Armstrong, M. Swinton, H. Ribberink, I. Beausoleil-Morrison and J. Millette, "Synthetically Derived Profiles for Representing Occupant-Driven Electric Loads

in Canadian Housing," Journal of Building Performance Simulation, vol. 2, no. 1, 2009.

[5] M. Carmo, D. Fritz, J. Mergel and D. Stolten, "A comprehensive reviwew on PEM water electrolysis," Int. Journal of Hydrogen Energy, pp. 4901-4934, 2013.

[6] F. Barbir, "PEM electrolysis for production of hydrogen from renewable energy sources," Solar Energy, vol. 78, pp. 661-669, 2005.

[7] J. Eichman, K. Harrison and M. Peters, "Novel Electrolyzer Applications: Providing more than just hydrogen," NREL, Denver, 2014.

[8] Y. Tang, W. Yuan, M. Pan and Z. Wan, "Experimental investigation on the dynamic performance of a hybrid PEM fuel cell/battery system for lightweight electric vehicle application," Applied Energy, vol. 88, no. 1, pp. 68-76, 2011.

[9] E. Costogue and R. Yasui, "Performance data for a terrestrial solar photovoltaie/water electrolysis experiment," Solar Energy, vol. 19, pp. 205-210, 1977.

[10] C. Carpetis, "A STUDY OF WATER ELECTROLYSIS WITH PHOTOVOLTAIC SOLAR ENERGY CONVERSION," Int. J. Hydrogen Energy, vol. 7, no. 4, pp. 287-310, 1982.

[11] P. Hollmuller, J.-M. Joubert, B. Lachal and K. Yvon, "Evaluation of a 5 kWp photovoltaic hydrogen production and storage installation for a residential home in Switzerland," International Journal of Hydrogen Energy, vol. 25, pp. 97-109, 2000.

[12] K. Voss, A. Goetzberger, G. Bopp, A. Haberle, A. Heinzel and H. Lehmberg, "The self-suffiecient solar house in Freiburg-Results of 3 years of operation," Solar Energy, vol. 58, pp. 17-23, 1996.

[13] Ø. Ulleberg and T. E. A. Nakken, "The wind/hydrogen demonstration system at Utsira in Norway: Evaluation of system performance using operational data and updated energy system modeling tools," Int. Journal of Hydrogen Energy, no. 35, pp. 1841-1852, 2010.

[14] W. De Soto, S. Klein and W. Beckman, "Improvement and validation of a model for photovoltaic array performance," Solar Energy, no. 80, pp. 78-88, 2006.

[15] Solar Energy Laboratory, University of Wisconsin-Madison, "TRNSYS 16 Mathematical Reference," University of Wisconsin-Madison, Madison, 2006.

[16] R. Garcia-Valverde, N. Espinosa and A. Urbina, "Simple PEM water electrolyser model and experimental," Int. Journal of Hydrogen Energy, no. 37, pp. 1927-1938, 2012.

[17] D. Fritz, J. Mergel and D. Stolten, "PEM electrolysis simulation and validation," in ECS Transactions, 2014.

[18] M. Schalenbach, M. Carmo, D. Fritz, J. Mergel and D. Stolten, "Pressurized PEM water electrolysis: Efficiency and gas crossover," Int. Journal of Hydrogen Energy, no. 38, pp. 14921-14933, 2013.

[19] O. P. Systems, "Outback Power," 2015. [Online]. Available: http://www.outbackpower.com/downloads/documents/energycell_re/energycellre_specsheet.pdf. [Accessed 8 January 2016].

[20] O. P. Systems, "Energy Cell Operating Manual," 2013. [Online]. Available: http://www.outbackpower.com/downloads/documents/energycell_re/energycell_manual.pdf. [Accessed 8 January 2016].

[21] A. Bergen, Integration and Dynamics of a Renewable Regenerative Hydrogen Fuel Cell System, Victoria: University of Victoria, 2008.

[22] Ø. Ulleberg, "Modeling of advanced alkaline electrolyzers: a system simulation approach," Int. Journal of Hydrogen Energy, no. 28, pp. 21-33, 2003.